
Backpropagation as Physical Relaxation: Exact Gradients in Finite Time

Antonino Emanuele Scurria¹

Abstract

Backpropagation, the foundational algorithm for training neural networks, is typically understood as a symbolic computation that recursively applies the chain rule. We show it emerges exactly as the finite-time relaxation of a physical dynamical system. By formulating feedforward inference as a continuous-time process and applying Lagrangian theory of non-conservative systems to handle asymmetric interactions, we derive a global energy functional on a doubled state space encoding both activations and sensitivities. The saddle-point dynamics of this energy perform inference and credit assignment simultaneously through local interactions. We term this framework “Dyadic Backpropagation”. Crucially, we prove that unit-step Euler discretization, the natural timescale of layer transitions, recovers standard backpropagation exactly in precisely $2L$ steps for an L -layer network, with no approximations. Unlike prior energy-based methods requiring symmetric weights, asymptotic convergence, or vanishing perturbations, our framework guarantees exact gradients in finite time. This establishes backpropagation as the digitally optimized shadow of a continuous physical relaxation, providing a rigorous foundation for exact gradient computation in analog and neuromorphic substrates where continuous dynamics are native.

1. Introduction

Standard neural network optimization relies on error Backpropagation (BP), an algorithm whose computational mechanism, as currently implemented and interpreted, is difficult to reconcile with physical reality. Specifically, it requires a backward pass topologically distinct from inference, the

¹Quantum Information Laboratory (LIQ) CP224, Université libre de Bruxelles (ULB), Av. F. D. Roosevelt 50, 1050 Bruxelles, Belgium. Correspondence to: Antonino Emanuele Scurria <antonino.scurria@ulb.be>.

Preprint. January 28, 2026.

transmission of non-local error signals, and synchronous global clocking (Crick, 1989). These constraints have no clear analog in physical systems, making backpropagation challenging to implement in neuromorphic hardware or biological models. Consequently, understanding how exact credit assignment can emerge from intrinsic system dynamics, through local interactions and continuous relaxation, remains a central open question.

Existing attempts to bridge this gap generally force a trade-off between physical realism and mathematical exactness. Equilibrium Propagation (Scellier & Bengio, 2017) frames learning as energy minimization but faces significant practical hurdles. Its reliance on a “nudging” phase yields only a gradient approximation and the constraint of symmetric weights (conservative systems and reciprocal forces) renders it fundamentally incompatible with modern feedforward architectures. Alternative approaches like Recurrent Backpropagation (Almeida, 1990; Pineda, 1987) require explicit, non-local error circuits, while Continuous Adjoint Methods (Chen et al., 2018a) rely on integrating dynamics backward in time—a process that is physically impossible for non-reciprocal systems like feedforward architectures. These examples highlight a pervasive tension in the field, where frameworks often struggle to be physically plausible without sacrificing mathematical exactness.

In this work, we propose a solution to this problem by demonstrating that standard backpropagation is neither an approximation nor a symbolic artifact, but the *exact* finite-time discrete trace of a continuous physical relaxation. By applying a modified version of the Lagrangian theory of non-conservative systems (Galley, 2013) (necessary to handle the asymmetric weights and interactions of feedforward networks), we construct a global energy functional on a doubled state space where the interaction between a ‘forward’ state and a ‘backward’ state mediates credit assignment.

- **Physical Unification:** We demonstrate that the algebraic steps of backpropagation emerge directly from Classical Mechanics, establishing a rigorous link between deep learning and physical laws.
- **Exactness in Finite Time:** We prove that the unit-step Euler discretization of this system recovers standard backpropagation exactly in $2L$ steps for an L -layer network,

interpreting BP as the digitally optimized implementation of a physical relaxation process.

- **Universality and Robustness:** Unlike prior methods limited by weight symmetry or vanishing perturbations, our framework naturally handles non-reciprocal dynamics and is architecture-agnostic. It is applicable to any computation graph differentiable via standard backpropagation, including CNNs and arbitrary feedforward topologies.

This establishes backpropagation as the digitally optimized shadow of a physical relaxation, providing a unified foundation for exact gradient computation in analog and neuromorphic substrates where continuous dynamics are native.

We term this framework Dyadic Backpropagation (DBP). It represents a variation of the dyadic dynamics proposed in (Scurria et al., 2026), here modified and specialized to accommodate feedforward systems.

2. Classical Backpropagation

This section establishes the notation and formal structure used throughout the paper.

2.1. Network Architecture

We consider a standard L -layer feedforward neural network with input $\mathbf{x}_0 \in \mathbb{R}^{n_0}$ and output $\mathbf{a}_L \in \mathbb{R}^{n_L}$. For each layer $\ell = 1, \dots, L$, the pre-activation and activation maps are respectively:

$$\begin{aligned} \mathbf{z}_\ell &= \mathbf{W}_\ell \mathbf{a}_{\ell-1} + \mathbf{b}_\ell, \\ \mathbf{a}_\ell &= \sigma_\ell(\mathbf{z}_\ell), \end{aligned} \quad (1) \quad (2)$$

where $\mathbf{W}_\ell \in \mathbb{R}^{n_\ell \times n_{\ell-1}}$, $\mathbf{b}_\ell \in \mathbb{R}^{n_\ell}$, and σ_ℓ is an elementwise nonlinearity. We collect all parameters into:

$$\theta = \{\mathbf{W}_\ell, \mathbf{b}_\ell\}_{\ell=1}^L.$$

2.2. Loss Function

A supervised loss function $C(\mathbf{a}_L, \mathbf{y})$ compares the network output to the target \mathbf{y} . Gradients of this loss with respect to parameters are computed via backpropagation.

2.3. Computing Gradients

Backpropagation(BP) computes gradients by introducing error vectors

$$\delta_\ell = \frac{\partial C}{\partial \mathbf{z}_\ell},$$

propagated recursively:

$$\delta_\ell = (\mathbf{W}_{\ell+1}^\top \delta_{\ell+1}) \odot \sigma'_\ell(\mathbf{z}_\ell),$$

with $\delta_L = \nabla_{\mathbf{a}_L} C \odot \sigma'_L(\mathbf{z}_L)$. Gradients follow:

$$\frac{\partial C}{\partial \mathbf{W}_\ell} = \delta_\ell \mathbf{a}_{\ell-1}^\top, \quad \frac{\partial C}{\partial \mathbf{b}_\ell} = \delta_\ell.$$

This layer-wise structure induces a strict ordering: gradients flow backward one layer at a time. We will reinterpret this process as a global dynamical system evolving under a single energy.

3. From Layers to Global Flow

We now move from the layer-wise discrete dynamics of classical backpropagation (Section 2) to a *global* description. The key step is to reinterpret the layer index as a discrete time coordinate and then embed this into a continuous-time vector field defined on a single stacked state. This will allow us to apply the Lagrangian theory of non-conservative systems to the network as a whole in Section 3.5.

3.1. Global Activation Vector

We start by stacking all layer activations into a single global state:

$$\mathbf{a} = \begin{bmatrix} \mathbf{a}_1 \\ \mathbf{a}_2 \\ \vdots \\ \mathbf{a}_L \end{bmatrix} \in \mathbb{R}^n, \quad n = \sum_{\ell=1}^L n_\ell. \quad (3)$$

This vector simply concatenates the activations at each hidden and output layer.

3.2. Block-Triangular Global Weight Matrix

Define the global weight matrix:

$$\mathbf{W} = \begin{bmatrix} \mathbf{0} & \mathbf{0} & \cdots & \mathbf{0} \\ \mathbf{W}_2 & \mathbf{0} & \cdots & \mathbf{0} \\ \vdots & \ddots & \ddots & \vdots \\ \mathbf{0} & \cdots & \mathbf{W}_L & \mathbf{0} \end{bmatrix}, \quad (4)$$

which is strictly lower block-triangular: information flows only from layer $\ell - 1$ to layer ℓ .

We collect all bias and input drives into the global vector

$$\boldsymbol{\beta}(\mathbf{x}_0) = \begin{bmatrix} \mathbf{W}_1 \mathbf{x}_0 + \mathbf{b}_1 \\ \mathbf{b}_2 \\ \vdots \\ \mathbf{b}_L \end{bmatrix}. \quad (5)$$

The forward pass over all layers can then be written compactly as the unique fixed point of

$$\mathbf{a} = \sigma(\mathbf{W}\mathbf{a} + \boldsymbol{\beta}(\mathbf{x}_0)), \quad (6)$$

where σ denotes the stacked nonlinearity acting elementwise.

3.3. The Forward Vector Field

In preparation for the energy-based formulation, we then proceed to generalize the feedforward dynamics from dis-

crete to continuous time as the fixed point of a global relaxation dynamics. We introduce a time-dependent global activation state $\mathbf{a}(t)$ evolving under the vector field

$$\frac{d\mathbf{a}(t)}{dt} = \sigma(\mathbf{W}\mathbf{a}(t) + \beta(\mathbf{x}_0)) - \mathbf{a}(t) =: F(\mathbf{a}(t)). \quad (7)$$

By construction, the equilibria of (7) are exactly the solutions of the fixed-point equation (6). In particular, the standard forward pass configuration corresponds to the unique stable equilibrium $\bar{\mathbf{a}}$ satisfying $\bar{\mathbf{a}} = \sigma(\mathbf{W}\bar{\mathbf{a}} + \beta(\mathbf{x}_0))$.

3.4. Nilpotency

It is useful to notice that in this global framework, the global connection matrix \mathbf{W} is strictly block lower-triangular and this implies a strong algebraic property.

Lemma 3.1 (Nilpotency of the Global Weight Matrix). *For an L -layer feedforward network, the global matrix \mathbf{W} satisfies:*

$$\mathbf{W}^L = \mathbf{0}.$$

Proof. Because \mathbf{W} has nonzero blocks only immediately below the diagonal, each multiplication by \mathbf{W} shifts nonzero contributions at most one block row down. After L such shifts, all contributions have moved past the last block row and vanish, hence $\mathbf{W}^L = \mathbf{0}$. \square

Nilpotency captures the acyclic structure of feedforward networks: information propagates strictly layer by layer with no feedback cycles. This property will imply finite-time convergence for the relaxation dynamics constructed in later sections.

3.5. Constructing the Global Energy

To construct a single global energy for the network, we must first address the fact that feedforward interactions are inherently *non-reciprocal*: information flows from layer ℓ to $\ell + 1$ without symmetric feedback. This violation of Newton's third law implies that the network vector field F previously defined in Eq. 7 is *non-conservative* and cannot be derived from a standard scalar potential (Goldstein et al., 2002).

To resolve this, we apply the Lagrangian theory of non-conservative systems. While inspired by the work of (Batemann, 1931) and (Galley, 2013), we modify the formalism to enable learning dynamics (see Appendix A). Crucially, to variationally encode non-reciprocal interactions, this theory entails a doubling of the phase space. We therefore introduce a conjugate pair of global state vectors: a “backward” state $\mathbf{x} \in \mathbb{R}^n$ and a “forward” state $\mathbf{z} \in \mathbb{R}^n$.

We embed the global vector field F into this generated coordinate system through a bilinear primal–dual coupling term, defining the global energy:

$$E(\mathbf{x}, \mathbf{z}) = \underbrace{(\mathbf{x} - \mathbf{z})^\top F\left(\frac{\mathbf{x} + \mathbf{z}}{2}\right)}_{\text{Lagrangian Lifting}} + \underbrace{C\left(\left[\frac{\mathbf{x} + \mathbf{z}}{2}\right]_L, \mathbf{y}\right)}_{\text{Cost}}. \quad (8)$$

Here the first term is a Lagrangian lifting of the vector field F into the doubled space, and the second term, the cost, injects task information solely through the midpoint's output block. The inclusion of the cost directly in the energy breaks the symmetry of the two states \mathbf{x} and \mathbf{z} with a perturbation that will encode the gradient (see Appendix A.3). Expanding the force term gives the explicit form

$$E(\mathbf{x}, \mathbf{z}) = (\mathbf{x} - \mathbf{z})^\top \left[\sigma\left(\mathbf{W}\frac{\mathbf{x} + \mathbf{z}}{2} + \beta(\mathbf{x}_0)\right) - \frac{\mathbf{x} + \mathbf{z}}{2} \right] + C\left(\left[\frac{\mathbf{x} + \mathbf{z}}{2}\right]_L, \mathbf{y}\right). \quad (9)$$

Interpretation.

- The midpoint $\frac{\mathbf{x} + \mathbf{z}}{2}$ is the activation value on which both the network dynamics and the loss are evaluated.
- The discrepancy $\mathbf{x} - \mathbf{z}$ encodes the gradient signal and stands for the deviation of the \mathbf{x} and \mathbf{z} states from the forward trajectory due to the perturbation through the cost function.

3.6. State Dynamics: A Tug-of-War for Credit

The equations of motion for the doubled system are governed by the variational principle of the underlying physical theory. Specifically, the formalism prescribes a saddle-point flow on the energy $E(\mathbf{x}, \mathbf{z})$ defined in Eq. (8), where the backward state \mathbf{x} ascends the energy while the forward state \mathbf{z} descends it:

$$\frac{d\mathbf{x}}{dt} = \frac{\partial E}{\partial \mathbf{x}}, \quad \frac{d\mathbf{z}}{dt} = -\frac{\partial E}{\partial \mathbf{z}}. \quad (10)$$

The resulting coupled dynamics are:

$$\begin{aligned} \frac{d\mathbf{x}}{dt} = & \underbrace{\left[\sigma\left(\mathbf{W}\frac{\mathbf{x} + \mathbf{z}}{2} + \beta(\mathbf{x}_0)\right) - \frac{\mathbf{x} + \mathbf{z}}{2} \right]}_{\text{Network Relaxation}} \\ & + \underbrace{\frac{1}{2} \left[\mathbf{W}^\top \text{diag}\left(\sigma'\left(\mathbf{W}\frac{\mathbf{x} + \mathbf{z}}{2} + \beta(\mathbf{x}_0)\right)\right) - \mathbf{I} \right] (\mathbf{x} - \mathbf{z})}_{\text{Backward Signal}} \\ & + \underbrace{\frac{1}{2} \begin{bmatrix} \mathbf{0} \\ \vdots \\ \nabla_{\mathbf{a}_L} C\left(\left[\frac{\mathbf{x} + \mathbf{z}}{2}\right]_L, \mathbf{y}\right) \end{bmatrix}}_{\text{Cost}}, \end{aligned} \quad (11)$$

and

$$\begin{aligned}
 \frac{dz}{dt} = & \underbrace{\left[\sigma\left(W \frac{x+z}{2} + \beta(x_0)\right) - \frac{x+z}{2} \right]}_{\text{Network Relaxation}} \\
 & - \underbrace{\frac{1}{2} \left[W^\top \text{diag}\left(\sigma'\left(W \frac{x+z}{2} + \beta(x_0)\right)\right) - I \right] (x-z)}_{\text{Backward Signal}} \\
 & - \underbrace{\frac{1}{2} \begin{bmatrix} 0 \\ \vdots \\ \nabla_{\mathbf{a}_L} C\left(\left[\frac{x+z}{2}\right]_L, \mathbf{y}\right) \end{bmatrix}}_{\text{Cost}}. \tag{12}
 \end{aligned}$$

These dynamics consist of three distinct physical forces:

The Network Relaxation: (first term in both equations) is identical for both states, driving x and z toward the forward pass configuration.

The Backward Signal: uses the stress $x - z$ to pull the states apart or push them together, mediated by the transpose of the linearized network dynamics to propagate error information.

The Cost: acts as an external force applied only to the output block of the network.

Crucially, this formalism requires identical initial conditions for both x and z . In this scenario, absent the cost term, both states collapse to the same dynamics, corresponding to the forward pass dynamics previously defined in section 3.3. Thus the cost is perturbing the system in order to encode the gradients in the stress term $(x - z)$ (see Appendix A.4).

3.7. Mean-Stress Variables

To better inspect the interaction between the two states x and z , it is useful to perform the following change of variable:

$$\mathbf{m} = \frac{1}{2}(x+z), \quad \mathbf{s} = x - z.$$

Differentiating the relations above yields the transformed system:

$$\begin{aligned}
 \frac{d\mathbf{m}}{dt} &= \sigma(W\mathbf{m} + \beta(x_0)) - \mathbf{m}, \\
 \frac{d\mathbf{s}}{dt} &= (W^\top D(\mathbf{m}) - I)\mathbf{s} + \nabla_{\mathbf{m}_L} C(\mathbf{m}_L, \mathbf{y}),
 \end{aligned} \tag{13}$$

where $D(\mathbf{m}) = \text{diag}(\sigma'(W\mathbf{m} + \beta(x_0)))$ is the diagonal matrix of local activation derivatives evaluated at the current mean state.

In this representation, the physical roles of the two variables become clear: \mathbf{m} relaxes toward a consistent forward activation pattern, while \mathbf{s} records the tension that enforces this consistency and channels sensitivity information backward through the network. It is also instructive to notice that, after the relaxation of \mathbf{m} , the energy of the system equals the task loss (see Appendix B).

3.8. The Equilibrium States

We now inspect the equilibria of the system in the \mathbf{m} , \mathbf{s} variables to better understand the configuration to which the system converges. The equilibria $\bar{\mathbf{m}}$ and $\bar{\mathbf{s}}$ satisfy the equilibrium equations:

$$\sigma(W\bar{\mathbf{m}} + \beta(x_0)) = \bar{\mathbf{m}} \tag{14}$$

$$(I - W^\top \bar{D})\bar{\mathbf{s}} = \nabla_{\bar{\mathbf{m}}_L} C(\bar{\mathbf{m}}_L, \mathbf{y}). \tag{15}$$

The first equation enforces the system to relax to the forward pass configurations. The second equation for $\bar{\mathbf{s}}$ yields exactly the same result as backpropagation (see Appendix C.1), where $\bar{\mathbf{s}}$ collects the total derivatives of the cost with respect to the equilibrium activations $\bar{\mathbf{m}}$:

$$\bar{\mathbf{s}}_\ell = \nabla_{\bar{\mathbf{m}}_\ell} C.$$

Stacking everything into a single vector yields

$$\bar{\mathbf{s}} = \begin{bmatrix} \nabla_{\bar{\mathbf{m}}_1} C \\ \nabla_{\bar{\mathbf{m}}_2} C \\ \vdots \\ \nabla_{\bar{\mathbf{m}}_L} C \end{bmatrix}. \tag{16}$$

The classical pre-activation errors are then obtained as

$$\Delta = \bar{D} \bar{\mathbf{s}} = \begin{bmatrix} \delta_1 \\ \delta_2 \\ \vdots \\ \delta_L \end{bmatrix}, \quad \delta_\ell = D_\ell(\bar{\mathbf{m}}_\ell) \bar{\mathbf{s}}_\ell, \tag{17}$$

where $D_\ell(\bar{\mathbf{m}}_\ell)$ is the diagonal derivative matrix at layer ℓ . Finally, one can easily check that this equilibrium configuration $(\bar{\mathbf{m}}, \bar{\mathbf{s}})$ is globally exponentially stable (see Appendix C.2).

3.9. Gradient Computation via the Adjoint Chain Rule

Now we use the equilibrium configuration of our system to compute the total derivative of the cost with respect to the weights, denoted $\nabla_W C$. Using the chain rule, the total gradient can be expressed in terms of the equilibrium variables:

$$\nabla_W C = \sum_j \nabla_{\bar{\mathbf{m}}_j} C \frac{\partial \bar{\mathbf{m}}_j}{\partial W} = \sum_j \bar{s}_j \frac{\partial (\sigma(W\bar{\mathbf{m}} + \beta))_j}{\partial W}. \tag{18}$$

Evaluating the partial derivative of the update rule $\bar{m}_i = \sigma_i(\sum_j W_{ij} \bar{m}_j + \beta_i)$ yields:

$$\frac{\partial \bar{m}_i}{\partial W_{ij}} = D_{ii}(\bar{\mathbf{m}}) \bar{m}_j, \tag{19}$$

where $D_{ii}(\bar{\mathbf{m}})$ denotes the i -th block of $\mathbf{D}(\bar{\mathbf{m}})$. Substituting this into (18), we obtain the standard gradient outer product:

$$\nabla_{\mathbf{W}} C = \Delta \bar{\mathbf{m}}^\top, \quad \Delta = \mathbf{D}(\bar{\mathbf{m}}) \bar{\mathbf{s}}. \quad (20)$$

In layer form, this recovers the familiar local gradients:

$$\nabla_{\mathbf{W}_\ell} C = \delta_\ell \bar{\mathbf{m}}_{\ell-1}^\top, \quad (21)$$

$$\nabla_{\mathbf{b}_\ell} C = \delta_\ell. \quad (22)$$

These expressions highlight the two-factor structure of gradient computation: a pre-synaptic activation $\bar{\mathbf{m}}_{\ell-1}$ and a post-synaptic variable δ_ℓ .

3.10. Dyadic Backpropagation Algorithm

After showing that this dynamics is yielding the exact gradient, we now present the algorithm implementing the learning dynamics (10). In this joint formulation in Algorithm 1, both states move on the same lattice at every time step.

Algorithm 1 Dyadic Backpropagation (DBP)

```

1: Input:  $\mathbf{x}_0, \mathbf{y}$ , parameters  $\{\mathbf{W}_\ell, \mathbf{b}_\ell\}_{\ell=1}^L$ , step size  $\eta > 0$ ,  

   tolerance  $\varepsilon > 0$ 
2: Initialize  $\mathbf{x}^0 = \mathbf{z}^0$ 
3: for  $k = 0, 1, 2, \dots$  do
4:    $\mathbf{m}^k \leftarrow \frac{1}{2}(\mathbf{x}^k + \mathbf{z}^k)$ 
5:    $\mathbf{D}^k \leftarrow \text{diag}(\sigma'(\mathbf{W}\mathbf{m}^k + \beta(\mathbf{x}_0)))$ 
6:   Compute loss gradient  $\mathbf{g}^k \leftarrow \nabla_{\mathbf{m}} C(\mathbf{m}^k, \mathbf{y})$ , embed-  

      ded on the output block
7:   Compute velocity fields from Eqs. (11), (12):  

       
$$\dot{\mathbf{x}}^k = \sigma(\mathbf{W}\mathbf{m}^k + \beta(\mathbf{x}_0)) - \mathbf{x}^k$$

       
$$+ \frac{1}{2}\mathbf{W}^\top \mathbf{D}^k(\mathbf{x}^k - \mathbf{z}^k) + \frac{1}{2}\mathbf{g}^k,$$

       
$$\dot{\mathbf{z}}^k = \sigma(\mathbf{W}\mathbf{m}^k + \beta(\mathbf{x}_0)) - \mathbf{z}^k$$

       
$$- \frac{1}{2}\mathbf{W}^\top \mathbf{D}^k(\mathbf{x}^k - \mathbf{z}^k) - \frac{1}{2}\mathbf{g}^k$$

8:   Update states by Euler integration:  

       
$$\mathbf{x}^{k+1} \leftarrow \mathbf{x}^k + \eta \dot{\mathbf{x}}^k, \quad \mathbf{z}^{k+1} \leftarrow \mathbf{z}^k + \eta \dot{\mathbf{z}}^k$$

9:   if  $\|\mathbf{x}^{k+1} - \mathbf{x}^k\|_2 + \|\mathbf{z}^{k+1} - \mathbf{z}^k\|_2 < \varepsilon$  then
10:    break
11:   end if
12: end for
13: Equilibrium variables:  

       
$$\bar{\mathbf{x}} = \mathbf{x}^k, \quad \bar{\mathbf{z}} = \mathbf{z}^k, \quad \bar{\mathbf{m}} = \frac{1}{2}(\bar{\mathbf{x}} + \bar{\mathbf{z}}), \quad \bar{\mathbf{s}} = \bar{\mathbf{x}} - \bar{\mathbf{z}}.$$

14: Gradient (equivalent to standard BP):  

       
$$\frac{dC}{d\mathbf{W}} = \mathbf{D}(\bar{\mathbf{m}}) \bar{\mathbf{s}} \bar{\mathbf{m}}^\top = \mathbf{D}\left(\frac{\bar{\mathbf{x}} + \bar{\mathbf{z}}}{2}\right) (\bar{\mathbf{x}} - \bar{\mathbf{z}}) \left(\frac{\bar{\mathbf{x}} + \bar{\mathbf{z}}}{2}\right)^\top.$$


```

The joint evolution of (\mathbf{x}, \mathbf{z}) in Algorithm 1 converges to the same saddle-point equilibrium as the two-phase mean, stress method in Eq. 13, and the resulting gradient will match the gradient of classical backpropagation as we have previously shown in section 3.9. Furthermore, a simplified dynamical scheme (see Appendix D) yielding identical accuracy has been developed for Algorithm 1 to facilitate hardware implementation.

4. The Discrete Trace: Recovering Backpropagation

We now study the discretized version of the continuous-time (\mathbf{m}, \mathbf{s}) dynamics Eq. (13) to explicitly show equivalence to the backpropagation dynamics.

4.1. Canonical Discretization and the Natural Time Step

Applying forward Euler with step size $\Delta t > 0$ to the equation 13 gives the discrete updates:

$$\mathbf{m}^{k+1} = \mathbf{m}^k + \Delta t [\sigma(\mathbf{W}\mathbf{m}^k + \beta(\mathbf{x}_0)) - \mathbf{m}^k], \quad (23)$$

$$\mathbf{s}^{k+1} = \mathbf{s}^k + \Delta t [(\mathbf{W}^\top \mathbf{D}(\mathbf{m}^k) - \mathbf{I}) \mathbf{s}^k + \nabla_{\mathbf{m}_L} C(\mathbf{m}_L^k, \mathbf{y})]. \quad (24)$$

Standard layer-by-layer backpropagation corresponds to choosing a *unit* Euler step, $\Delta t = 1$. This specific choice acts as a dead-beat gain: it exactly cancels the inertial term $(1 - \Delta t)\mathbf{m}^k$. In that case, the equations simplify to the coupled map:

$$\mathbf{m}^{k+1} = \sigma(\mathbf{W}\mathbf{m}^k + \beta(\mathbf{x}_0)), \quad (25)$$

$$\mathbf{s}^{k+1} = \mathbf{W}^\top \mathbf{D}(\mathbf{m}^k) \mathbf{s}^k + \nabla_{\mathbf{m}_L} C(\mathbf{m}_L^k, \mathbf{y}). \quad (26)$$

4.2. Nilpotency and Exact Convergence in 2L Steps

We now show that we obtain finite time convergence of the discretized dynamical equations (25)(26) in exactly $2L$ steps, where L corresponds to the depth of the network as before. This can be easily seen because \mathbf{W} is strictly lower block-triangular. Then each block \mathbf{m}_ℓ depends only on upstream layers $\mathbf{m}_1, \dots, \mathbf{m}_{\ell-1}$, ensuring strictly sequential convergence.

Lemma 4.1 (Forward Layer Freezing). *For the iteration (25) with initial condition \mathbf{m}^0 , the ℓ -th block satisfies*

$$\mathbf{m}_\ell^k = \mathbf{a}_\ell \quad \text{for all } k \geq \ell,$$

where \mathbf{a}_ℓ denotes the standard forward activation at layer ℓ .

Proof. The proof proceeds by induction on ℓ . For $\ell = 1$, the update reads

$$\mathbf{m}_1^{k+1} = \sigma_1(\mathbf{W}_1 \mathbf{x}_0 + \mathbf{b}_1),$$

which is independent of k ; hence $\mathbf{m}_1^k = \mathbf{a}_1$ for all $k \geq 1$. Now assume the claim holds for layers $1, \dots, \ell - 1$. The ℓ -th block update uses only $\mathbf{m}_{\ell-1}^k$, which equals $\mathbf{a}_{\ell-1}$ for all $k \geq \ell - 1$. Thus for $k \geq \ell - 1$,

$$\mathbf{m}_\ell^{k+1} = \sigma_\ell(\mathbf{W}_\ell \mathbf{m}_{\ell-1}^k + \mathbf{b}_\ell) = \sigma_\ell(\mathbf{W}_\ell \mathbf{a}_{\ell-1} + \mathbf{b}_\ell) = \mathbf{a}_\ell,$$

and the claim follows. \square

Let $\bar{\mathbf{m}}$ denote the stacked forward activations at equilibrium. It follows that for all $k \geq L$, $\mathbf{m}^k = \bar{\mathbf{m}}$. Thus the forward relaxation converges in exactly L iterations.

We now need to inspect the convergence of the \mathbf{s} variable.

Crucially, the \mathbf{s} update in Eq. (26) uses the matrix $\mathbf{D}(\mathbf{m}^k)$. We can then use the fact that for $k \geq L$ we get

$$\mathbf{D}(\mathbf{m}^k) = \mathbf{D}(\bar{\mathbf{m}}) =: \bar{\mathbf{D}}, \quad \text{for all } k \geq L.$$

Consequently, for all subsequent steps $k \geq L$, the update for \mathbf{s} becomes a linear dynamical system with a *constant* transition matrix $\bar{\mathbf{M}} = \mathbf{W}^\top \bar{\mathbf{D}}$:

$$\mathbf{s}^{k+1} = \bar{\mathbf{M}} \mathbf{s}^k + \nabla C, \quad \text{for } k \geq L.$$

The convergence of this phase relies on the algebraic properties of $\bar{\mathbf{M}}$. Because the network is feedforward, $\bar{\mathbf{M}}$ is strictly upper block-triangular and thus *nilpotent* with index L (i.e., $\bar{\mathbf{M}}^L = \mathbf{0}$).

This nilpotency guarantees that any transient (or residual) information accumulated in \mathbf{s} during the initial transient phase (steps 0 to $L-1$, when \mathbf{D} is changing) is progressively shifted out of the network. After exactly L applications of the constant operator $\bar{\mathbf{M}}$ (i.e., at step $k = L + L = 2L$), the memory of the initial transient is completely annihilated, and the state settles exactly into the fixed point previously discussed (see Eq. 16).

More formally:

Theorem 4.2 (Autonomous Finite-Time Convergence). *Let the coupled system evolve simultaneously through Equations 25 and 26. Then:*

1. **Forward Settling** ($k \leq L$): *The primal state converges to the valid network activations at $k = L$, i.e., $\mathbf{m}^k = \bar{\mathbf{m}}$ for all $k \geq L$.*
2. **Backward Flushing** ($L < k \leq 2L$): *With \mathbf{m} fixed, the dual state flushes out transient errors and converges to the exact backpropagation gradients at $k = 2L$, i.e., $\mathbf{s}^k = \bar{\mathbf{s}}$ for all $k \geq 2L$.*

Thus, the system solves the backpropagation problem autonomously in $2L$ steps without external mode switching.

Writing then the corresponding dynamics in algorithmic form we get:

Algorithm 2 Dynamical Backpropagation

```

1: Input:  $\mathbf{x}_0, \mathbf{y}, \{\mathbf{W}_\ell, \mathbf{b}_\ell\}_{\ell=1}^L$ 
2: Initialize:  $\mathbf{m}^0, \mathbf{s}^0$ 
3: // Simultaneous evolution loop
4: for  $k = 0$  to  $2L - 1$  do
5:    $\mathbf{m}^{k+1} \leftarrow \sigma(\mathbf{W} \mathbf{m}^k + \beta(\mathbf{x}_0))$ 
6:    $\mathbf{D}^k \leftarrow \text{diag}(\sigma'(\mathbf{W} \mathbf{m}^k + \beta(\mathbf{x}_0)))$ 
7:    $\mathbf{s}^{k+1} \leftarrow \mathbf{W}^\top \mathbf{D}^k \mathbf{s}^k + \nabla_{\mathbf{m}_L} C(\mathbf{m}_L^k, \mathbf{y})$ 
8: end for
9: Gradient:  $\frac{\partial C}{\partial \mathbf{W}} = \mathbf{D}(\mathbf{m}^{2L}) \mathbf{s}^{2L} (\mathbf{m}^{2L})^\top$ 

```

Together, Theorem 4.2 and Algorithm 2 establish that standard backpropagation is the exact discrete trace of the continuous \mathbf{x} – \mathbf{z} saddle-point dynamics in Eq. 10. The conventional two-phase procedure of the forward and backward passes is thus revealed to be a computational optimization of this single physical process, skipping redundant updates during the system’s natural settling phases (we stop updating \mathbf{m} as soon as it settles to its equilibrium). Consequently, the familiar forward and backward passes are not arbitrary engineering choices, but the intrinsic relaxation behaviors of the underlying physical system.

5. Empirical Validation

We empirically validate Dyadic Backpropagation (DBP) (Algorithm 1) on CIFAR-10, comparing its performance and internal dynamics against standard backpropagation (BP).

5.1. Setup

Architecture. We employ a 9-layer VGG-style CNN ($\sim 5M$ parameters) comprising four convolutional blocks (Conv-ReLU-Conv-ReLU-Stride2Pool) with channel dimensions [64, 128, 256, 512], followed by a linear classifier.

Training. Models are trained for 100 epochs with a batch size of 64 using SGD with Nesterov momentum ($\mu = 0.9$), weight decay (5×10^{-4}), and cosine learning rate annealing ($0.035 \rightarrow 0.0002$). We apply standard data augmentation (random crops, horizontal flips, Cutout) and label smoothing ($\epsilon = 0.1$) consistently across all experiments.

Relaxation Parameters. We investigate the Euler step size $\eta \in \{0.25, 0.50, 0.75, 1.00\}$, allowing up to $K_{\max} = 1000$ relaxation iterations per training step. Early stopping is triggered when the difference (Euclidean norm) between successive iterations is smaller than 10^{-6} . All runs use

identical random seeds to ensure fair comparison.

Metrics. We evaluate gradient fidelity by comparing the relaxation-derived gradients ∇_{relax} against reference gradients ∇_{BP} computed via automatic differentiation. Key metrics include (additional metrics in Appendix E):

- **Cosine similarity:** $\text{CosSim} = \frac{\langle \nabla_{\text{relax}}, \nabla_{\text{BP}} \rangle}{\|\nabla_{\text{relax}}\| \|\nabla_{\text{BP}}\|}$
- **Relative error:** $\frac{\|\nabla_{\text{relax}} - \nabla_{\text{BP}}\|}{\|\nabla_{\text{BP}}\|}$
- **Layer-wise alignment:** Per-layer cosine similarity to analyze signal propagation depth.

Code and Reproducibility. All experiments are implemented in PyTorch. Code with fixed random seeds is provided in the supplementary material to ensure reproducibility.

5.2. Results

Our experiments confirm the theoretical predictions, demonstrating that the proposed method achieves robust stability across a wide range of step sizes, consistent with theoretical bounds.

Generalization Performance. As shown in Figure 1, the choice of the discretization step size η in Algorithm 1 does not negatively impact the learning trajectory. Algorithm 1 achieves test accuracy parity with standard Backpropagation (BP), reaching a peak of roughly 93%. This indicates that the discrete-time saddle-point dynamics successfully approximate the learning signal of the ideal gradient.

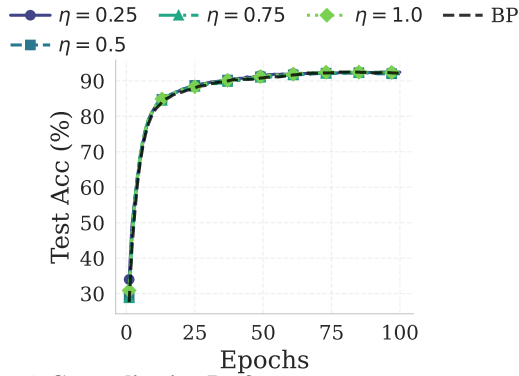


Figure 1. Generalization Performance. Test accuracy evolution for varying step sizes η matches the BP baseline (dashed black), reaching $\sim 93\%$.

Gradient Fidelity and Dynamics. Beyond generalization accuracy, we analyze the internal mechanics of the method. Figure 2 corroborates our core theoretical claims:

- **Precision (left panel):** The algorithm recovers the true gradient parameters with high accuracy, as indicated by

the low global relative error. As detailed in Appendix E.2, this residual error is driven almost entirely by a mismatch in Euclidean norms rather than directional deviation. In fact, we will see the directional misalignment is negligible, remaining barely indistinguishable from machine precision.

- **Convergence Speed (central Panel):** We observe a direct relationship between step size and relaxation efficiency. As the step size $\eta \rightarrow 1$, the number of required relaxation steps collapses toward the theoretical lower bound of $2L = 18$ (twice the network depth).

- **Alignment (right panel):** Layer-wise analysis reveals high-fidelity alignment across all layers. To visualize deviations, we plot the log-misalignment $\log_{10}(1 - \cos \theta)$. The heatmap demonstrates that errors generally hover near the IEEE 754 Float32 machine precision limit ($\approx 10^{-7}$), making the physical relaxation basically indistinguishable from the symbolic algorithm for most practical purposes. Additional details can be found in E.5.

In sum, these results confirm that Algorithm 1 reliably recovers the exact gradients of standard backpropagation. This validates the central thesis that the relaxation process is not an approximation, but the faithful continuous-time generator of the discrete backpropagation update. Further experiments corroborating the accuracy of the method can be found in Appendix E.

6. Related Work

Our work connects to a broad literature interpreting backpropagation through dynamical and energy-based lenses. Below, we distinguish our formulation from prior approaches.

- **Contrastive Hebbian Learning & Equilibrium Prop.** CHL (Movellan, 1991) and Equilibrium Propagation (Scellier & Bengio, 2017) rely on vanishing perturbations ($\beta \rightarrow 0$) or symmetric weights. They recover gradients only as a limiting process and are unable to yield the analytically exact gradient.
- **Recurrent Backpropagation (RBP).** RBP (Almeida, 1990; Pineda, 1987) computes gradients via a separate linear fixed-point equation for error signals. Unlike our variational framework, where both forward and backward dynamics emerge from a single energy functional through the physical principle of least action, RBP constructs the backward phase as an auxiliary adjoint system engineered specifically for gradient computation.
- **Predictive Coding.** Predictive coding (Rao & Ballard, 1999) approximates backprop via local error propagation. These methods generally require weight symmetry or linearization and typically recover exact gradients only in the limit of vanishing perturbations (weak nudging).

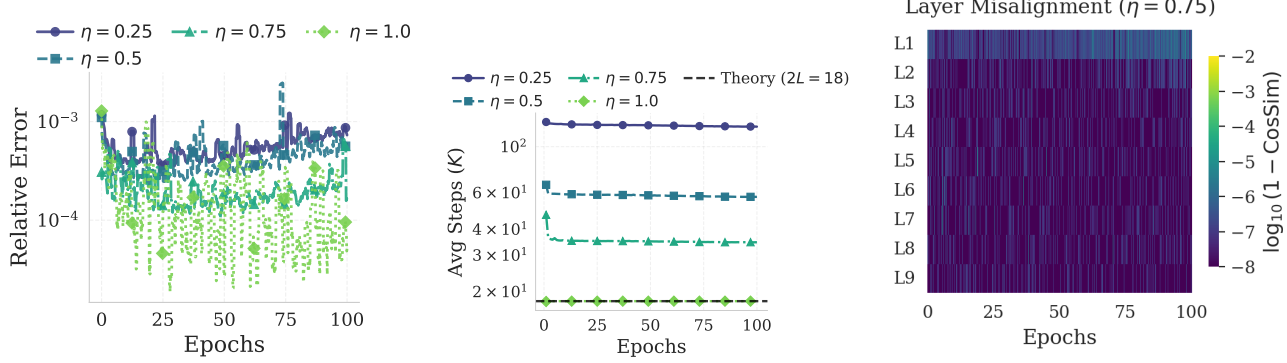


Figure 2. Empirical Validation of Dynamics. (left) **Relative gradient error** shows accurate recovery of ∇_{BP} . (center) **Relaxation steps** converge to the theoretical limit $2L = 18$ as $\eta \rightarrow 1$. (right) **Log-misalignment heatmap** ($\eta = 0.75$) plots $\log_{10}(1 - \text{CosSim})$ for each layer L_i . Values hover between -6 and -8 , bounded by IEEE 754 Float32 machine precision ($\approx 10^{-7}$), rendering relaxation gradients basically indistinguishable from BP.

- **Adjoint ODE Methods.** Continuous-time adjoints (Chen et al., 2018b) require integrating backwards in time, a process that is physically impossible for dissipative and non-reciprocal systems. Furthermore, they match discrete backpropagation only in the limit of infinitesimal step sizes. Our method avoids reverse-time integration and recovers the exact algebraic updates of standard networks through discrete forward-time relaxation in finite steps.
- **Method of Auxiliary Coordinates (MAC).** MAC (Carreira-Perpinan & Wang, 2014) enforces layer-wise consistency via quadratic penalties, achieving exact gradients only in the limit of infinite penalty weights.
- **Target Propagation.** Target propagation (Bengio, 2020) relies on approximating layer inverses to propagate signals. This approach faces fundamental limitations when layers are lossy or non-invertible (e.g., ReLUs), making it difficult to recover exact gradients. Our dual dynamics bypass the need for explicit inversion entirely, handling these non-linearities implicitly to recover standard backpropagation exactly.
- **Dual Propagation.** Dual propagation (Høier et al., 2023) explicitly postulates a doubled state representation to facilitate error encoding within a Contrastive Hebbian Learning framework. However, as an energy-based approach, it relies on weight symmetry and recovers exact gradients only asymptotically in the weak feedback limit. In contrast, our dual variables emerge naturally from the Lagrangian formulation of the network dynamics, enabling a framework that inherently supports asymmetric weights and yields exact gradients in finite time.

Summary. Unlike methods that rely on asymptotic limits ($\beta \rightarrow 0$), infinite penalties, biased approximations, or explicitly engineered error circuits, Dyadic Backpropagation derives a *single variational dynamical system*. This system does not merely approximate the gradient; it reveals standard backpropagation as the exact **discrete-time projection**

of a continuous physical relaxation.

7. Conclusion

As deep learning models scale, the energy and synchronization costs of digital von Neumann architectures are becoming a fundamental bottleneck. This work offers a theoretical path to transcend these limitations. By proving that standard backpropagation emerges from physical laws as the exact discrete trace of a continuous relaxation dynamics, we demonstrate that gradient computation does not inherently require global clocks, symbolic differentiation, or rigid algorithmic phasing.

Instead, we have shown that learning can be reformulated as a purely physical process: the resolution of "stress" between a forward state and a backward state. This perspective implies that the computational heavy lifting of credit assignment can be offloaded to the natural equilibrium dynamics of the substrate itself. Furthermore, we observe that this derivation is reminiscent of multi-compartment cortical neuron models, where apical dendrites integrate feedback signals separately from basal feedforward inputs (Guerguiev et al., 2017), suggesting that our framework may bridge not only digital and analog computing, but also artificial and biological learning.

Consequently, this work provides a rigorous foundation for a new class of analog and neuromorphic hardware where learning is driven by local physical processes rather than centralized arithmetic. By bridging the gap between the discrete mathematics of the chain rule and the continuous reality of physics, we provide a theoretical foundation for systems where the hardware does not merely execute the algorithm, but physically embodies it.

Acknowledgments

AES acknowledges financial support from the Horizon Europe Marie Skłodowska-Curie Doctoral Network ‘Postdigital Plus’ (Grant 101169118). AES also thanks Serge Massar, Dimitri Vanden Abeele, Bortolo Matteo Mognetti, and Alessandro Salvatore for fruitful discussions and valuable suggestions. Computational resources have been provided by the Consortium des Équipements de Calcul Intensif (CÉCI), funded by the Fonds de la Recherche Scientifique de Belgique (F.R.S.-FNRS) under Grant No. 2.5020.11 and by the Walloon Region.

“*Vanitas vanitatum et omnia vanitas*”

References

Almeida, L. B. A learning rule for asynchronous perceptrons with feedback in a combinatorial environment. In *Artificial neural networks: concept learning*, pp. 102–111. 1990.

Bateman, H. On dissipative systems and related variational principles. *Physical Review*, 38(4):815, 1931.

Bengio, Y. Deriving differential target propagation from iterating approximate inverses. *arXiv preprint arXiv:2007.15139*, 2020.

Carreira-Perpinan, M. and Wang, W. Distributed optimization of deeply nested systems. pp. 10–19, 2014.

Chen, R. T., Rubanova, Y., Bettencourt, J., and Duvenaud, D. K. Neural ordinary differential equations. *Advances in neural information processing systems*, 31, 2018a.

Chen, R. T. Q., Rubanova, Y., Bettencourt, J., and Duvenaud, D. Neural ordinary differential equations. 2018b.

Crick, F. The recent excitement about neural networks. *Nature*, 337, 1989.

Galley, C. R. Classical mechanics of nonconservative systems. *Physical review letters*, 110(17):174301, 2013.

Goldstein, H., Poole, C., and Safko, J. *Classical Mechanics*. Addison Wesley, 3rd edition, 2002.

Guerguiev, J., Lillicrap, T. P., and Richards, B. A. Towards deep learning with segregated dendrites. *elife*, 6:e22901, 2017.

Høier, R., Staudt, D., and Zach, C. Dual propagation: accelerating contrastive hebbian learning with dyadic neurons. In *Proceedings of the 40th International Conference on Machine Learning*, ICML’23. JMLR.org, 2023.

Movellan, J. R. Contrastive hebbian learning in the continuous hopfield model. In *Connectionist models*, pp. 10–17. Elsevier, 1991.

Pineda, F. Generalization of back propagation to recurrent and higher order neural networks. In *Neural information processing systems*, 1987.

Rao, R. P. and Ballard, D. H. Predictive coding in the visual cortex: a functional interpretation of some extra-classical receptive-field effects. *Nature Neuroscience*, 2:79–87, 1999.

Scellier, B. and Bengio, Y. Equilibrium propagation: Bridging the gap between energy-based models and backpropagation. *Frontiers in computational neuroscience*, 11:24, 2017.

Scurria, A. E., Vanden Abeele, D., Mognetti, B. M., and Massar, S. Equilibrium propagation for non-conservative systems. In preparation, 2026.

A. Overview on Out-of-Equilibrium Mechanics

This appendix provides a brief overview of the classical mechanics of non-conservative systems to motivate the definition of the global energy functional $E(\mathbf{x}, \mathbf{z})$ presented in Eq. 8. Our construction draws on the formalism developed by (Galley, 2013) and (Bateman, 1931), adapted here for the specific context of neural dynamics.

A.1. The Inverse Problem of Variation

The fundamental challenge in formulating a physical theory of backpropagation is that neural networks are inherently *non-reciprocal* systems. The information flows from layer ℓ to $\ell + 1$, but not vice versa. Mathematically, if we view the network update as a vector field $\dot{\mathbf{u}} = F(\mathbf{u})$, the Jacobian matrix ∇F is strictly block-lower triangular and thus asymmetric.

From the inverse problem of the calculus of variations (the Helmholtz conditions), we know that a vector field $F(\mathbf{u})$ can be represented as the gradient of a scalar potential H (i.e., $F = -\nabla H$) if and only if its Jacobian is symmetric (self-adjoint). Since the network dynamics are non-reciprocal, they contain a non-vanishing “rotational” component, meaning no single scalar potential $H(\mathbf{u})$ exists whose gradient generates the feedforward dynamics.

A.2. The Galley Formalism and the Decomposition Bottleneck

To address non-conservative forces, (Galley, 2013) introduces a doubled action principle. The general action S on the paths $\mathbf{z}(t)$ (forward) and $\mathbf{x}(t)$ (backward) is defined as:

$$S[\mathbf{x}, \mathbf{z}] = \int_{t_i}^{t_f} [\mathcal{L}(\mathbf{x}, \dot{\mathbf{x}}) - \mathcal{L}(\mathbf{z}, \dot{\mathbf{z}}) + K(\mathbf{x}, \mathbf{z})] dt, \quad (27)$$

where \mathcal{L} accounts for the conservative (potential-derived) dynamics, and $K(\mathbf{x}, \mathbf{z})$ is a non-conservative potential that couples the two paths.

Strict application of this formalism requires decomposing the force field $F(\mathbf{u})$ into a conservative gradient part (absorbed into \mathcal{L}) and a non-conservative rotational part (assigned to K). Mathematically, this corresponds to a **Helmholtz-Hodge decomposition** of the network vector field. For deep neural networks, computing this decomposition explicitly is computationally intractable, as it requires isolating the integrable component of the high-dimensional network dynamics.

A.3. Constructing the Global Energy

To circumvent this difficulty, we propose a modification to the standard approach. Rather than attempting to isolate

a conservative potential, we treat the *entire* vector field $F(\mathbf{u})$, including any potentially conservative linear parts, as a generalized non-conservative force.

We construct a single global interaction energy E_{int} that embeds the full vector field F directly into the bilinear coupling term:

$$E_{\text{int}}(\mathbf{x}, \mathbf{z}) = (\mathbf{x} - \mathbf{z})^\top F \left(\frac{\mathbf{x} + \mathbf{z}}{2} \right). \quad (28)$$

This specific bilinear form is designed to act as a *generator* for the complete vector field F , rendering the explicit decomposition unnecessary. We prescribe the equations of motion as a saddle-point flow on this energy:

$$\dot{\mathbf{x}} = \frac{\partial E_{\text{int}}}{\partial \mathbf{x}}, \quad \dot{\mathbf{z}} = -\frac{\partial E_{\text{int}}}{\partial \mathbf{z}}. \quad (29)$$

Evaluating these gradients yields the explicit dynamics:

$$\dot{\mathbf{x}} = F(\mathbf{m}) + \frac{1}{2} [\nabla F(\mathbf{m})]^\top (\mathbf{x} - \mathbf{z}), \quad (30)$$

$$\dot{\mathbf{z}} = F(\mathbf{m}) - \frac{1}{2} [\nabla F(\mathbf{m})]^\top (\mathbf{x} - \mathbf{z}), \quad (31)$$

where $\mathbf{m} = \frac{1}{2}(\mathbf{x} + \mathbf{z})$.

Crucially, on the physical submanifold where $\mathbf{x} = \mathbf{z}$ (i.e., zero stress), the coupling terms containing $[\nabla F]^\top (\mathbf{x} - \mathbf{z})$ vanish identically. On this manifold, both equations collapse to the exact target dynamics:

$$\dot{\mathbf{x}} = \dot{\mathbf{z}} = F(\mathbf{x}). \quad (32)$$

This formulation allows us to apply the doubled-variable framework to arbitrary network architectures without requiring the prohibitive Hodge decomposition.

A.4. Symmetry Breaking as Credit Assignment

The variational principle established above successfully generates the forward dynamics on the diagonal manifold $\mathbf{x} = \mathbf{z}$. On this manifold, the system possesses a gauge symmetry: the forward state \mathbf{z} is redundant, and the stress $(\mathbf{x} - \mathbf{z})$ is zero.

We propose to exploit this symmetry to perform credit assignment. Specifically, we introduce the task loss $C(\mathbf{m})$ as a symmetry-breaking potential acting on the output block. By adding this cost to the global energy, we intentionally perturb the gauge symmetry of the system.

This perturbation exerts opposite forces on the pair: it drives \mathbf{z} to descend the loss landscape (energy minimization) while forcing \mathbf{x} to ascend the constraint violations (energy maximization).

This "tug-of-war" induces a physical separation $\mathbf{s} = \mathbf{x} - \mathbf{z}$. The evolution of this stress variable follows the difference

of the velocity fields:

$$\dot{\mathbf{s}} = \dot{\mathbf{x}} - \dot{\mathbf{z}} = [\nabla F(\mathbf{m})]^\top \mathbf{s} + \nabla C. \quad (33)$$

This naturally recovers the exact adjoint equation. Thus, in our framework, backpropagation emerges not as a symbolic operation, but as the physical relaxation of the stress induced by explicitly breaking the symmetry of the forward pass.

B. Equilibrium energy equals task loss.

It is instructive to compute the value of the specific energy $E(\mathbf{m}, \mathbf{s})$ at the equilibrium point $(\bar{\mathbf{m}}, \bar{\mathbf{s}})$. In the forward phase, the primal variable \mathbf{m} relaxes to the exact fixed point of the network equations:

$$\bar{\mathbf{m}} = \sigma(\mathbf{W}\bar{\mathbf{m}} + \beta(\mathbf{x}_0)). \quad (34)$$

Substituting this into the energy equation (9), the first term (the constraint violation) vanishes identically:

$$E(\bar{\mathbf{m}}, \bar{\mathbf{s}}) = \bar{\mathbf{s}}^\top \underbrace{[\sigma(\mathbf{W}\bar{\mathbf{m}} + \beta(\mathbf{x}_0)) - \bar{\mathbf{m}}]}_0 + C(\bar{\mathbf{m}}_L, \mathbf{y}) \quad (35)$$

$$= C(\bar{\mathbf{m}}_L, \mathbf{y}). \quad (36)$$

This result confirms that the saddle-point equilibrium is physically meaningful: the "stored work" in the constraints $(\mathbf{s}^\top [\dots])$ vanishes when the forward pass is valid, leaving only the potential energy of the output error. The system thus relaxes to a state where the energy is exactly the task loss, constrained to the manifold of valid network activations.

C. Properties of the Equilibrium

In this section we analyze some claims of the main text related to the properties of the equilibrium configuration of our relaxation dynamics.

C.1. Explicit Equivalence to Backpropagation

We derive the explicit form of the equilibrium state $\bar{\mathbf{s}}$ by directly inverting the linear system governing the backward phase. Recall the equilibrium condition for the stress variable from Eq. (15):

$$(\mathbf{I} - \mathbf{W}^\top \bar{\mathbf{D}}) \bar{\mathbf{s}} = \nabla_{\mathbf{m}} C, \quad (37)$$

where $\nabla_{\mathbf{m}} C$ denotes the gradient of the loss with respect to all activations. Due to the network structure, this vector is sparse, containing non-zero entries only in the block corresponding to the output layer L .

Let $\mathbf{M} = \mathbf{W}^\top \bar{\mathbf{D}}$. Since \mathbf{W} is strictly lower block-triangular (representing feedforward connectivity), its transpose \mathbf{W}^\top is strictly upper block-triangular. The multiplication by the diagonal matrix $\bar{\mathbf{D}}$ preserves this structure.

Consequently, \mathbf{M} acts as a “backward shift” operator, moving signals from layer ℓ to $\ell - 1$. Crucially, this implies that \mathbf{M} is nilpotent with index L :

$$\mathbf{M}^L = \mathbf{0}. \quad (38)$$

Physically, this reflects the fact that error signals cannot propagate backward through more than L layers.

Because \mathbf{M} is nilpotent, the matrix $(\mathbf{I} - \mathbf{M})$ is invertible, and its inverse is given exactly by the finite Neumann series:

$$(\mathbf{I} - \mathbf{M})^{-1} = \sum_{k=0}^{L-1} \mathbf{M}^k = \mathbf{I} + \mathbf{M} + \mathbf{M}^2 + \cdots + \mathbf{M}^{L-1}. \quad (39)$$

Substituting this into the equilibrium equation yields the closed-form solution:

$$\bar{\mathbf{s}} = \left(\sum_{k=0}^{L-1} (\mathbf{W}^\top \bar{\mathbf{D}})^k \right) \nabla_{\mathbf{m}} C. \quad (40)$$

Interpretation. This series expansion recovers the standard backpropagation of errors. The term $k = 0$ captures the direct loss gradient at the output. The term $k = 1$ represents the loss gradient backpropagated by one layer $(\mathbf{W}^\top \bar{\mathbf{D}} \nabla_{\mathbf{m}} C)$, and the general term k represents the contribution of the loss backpropagated through k layers. Since $\nabla_{\mathbf{m}} C$ is non-zero only at layer L , the vector $\bar{\mathbf{s}}$ correctly aggregates the total derivative of the loss with respect to the activations at every layer ℓ .

C.2. Exponential Stability of the Equilibrium

We analyze the local stability of the coupled dynamical system by inspecting the spectrum of its Jacobian matrix at the equilibrium point $(\bar{\mathbf{m}}, \bar{\mathbf{s}})$.

Let $\mathbf{u} = [\mathbf{m}^\top, \mathbf{s}^\top]^\top$ denote the full state vector. The total Jacobian $\mathcal{J} \in \mathbb{R}^{2n \times 2n}$ is given by the block matrix:

$$\mathcal{J} = \begin{bmatrix} \frac{\partial \dot{\mathbf{m}}}{\partial \mathbf{m}} & \frac{\partial \dot{\mathbf{m}}}{\partial \mathbf{s}} \\ \frac{\partial \dot{\mathbf{s}}}{\partial \mathbf{m}} & \frac{\partial \dot{\mathbf{s}}}{\partial \mathbf{s}} \end{bmatrix}. \quad (41)$$

From the system definition in Eq. (13), we observe that the evolution of the primal variable \mathbf{m} is independent of the dual variable \mathbf{s} . Consequently, the upper-right block vanishes:

$$\frac{\partial \dot{\mathbf{m}}}{\partial \mathbf{s}} = \mathbf{0}.$$

This block-triangular structure implies that the spectrum of \mathcal{J} is the union of the spectra of its diagonal blocks. We analyze them individually:

1. Primal Block (\mathbf{m}). The linearization of the forward dynamics is

$$\mathbf{J}_{\mathbf{m}\mathbf{m}} = \frac{\partial \dot{\mathbf{m}}}{\partial \mathbf{m}} = \text{diag}(\sigma'(\mathbf{m})) \mathbf{W} - \mathbf{I}.$$

Since \mathbf{W} is strictly lower block-triangular (nilpotent), the product $\text{diag}(\dots) \mathbf{W}$ retains this strictly lower triangular structure and has zeros on its main diagonal. Therefore, the eigenvalues are determined solely by the identity term:

$$\text{spec}(\mathbf{J}_{\mathbf{m}\mathbf{m}}) = \{-1\}.$$

2. Dual Block (\mathbf{s}). The linearization of the backward dynamics with respect to \mathbf{s} is

$$\mathbf{J}_{\mathbf{s}\mathbf{s}} = \frac{\partial \dot{\mathbf{s}}}{\partial \mathbf{s}} = \mathbf{W}^\top \text{diag}(\sigma'(\mathbf{m})) - \mathbf{I}.$$

Since \mathbf{W} is strictly lower triangular, its transpose \mathbf{W}^\top is strictly upper triangular. The product $\mathbf{W}^\top \text{diag}(\dots)$ is thus strictly upper triangular with a zero diagonal. Similarly, the eigenvalues are determined by the identity term:

$$\text{spec}(\mathbf{J}_{\mathbf{s}\mathbf{s}}) = \{-1\}.$$

Conclusion. The Jacobian \mathcal{J} has a single eigenvalue $\lambda = -1$ with algebraic multiplicity $2n$. Since $\text{Re}(\lambda) < 0$, the equilibrium $(\bar{\mathbf{m}}, \bar{\mathbf{s}})$ is **globally exponentially stable**. The system relaxes with a natural time constant $\tau = 1$, ensuring rapid convergence to the backpropagation solution regardless of initialization. Finally, the (\mathbf{x}, \mathbf{z}) system also possesses globally exponentially stable equilibria, given that these dynamics are obtained are obtained through a linear change of variable.

D. Alternative Formulation: Split-Dynamics

To facilitate implementation on hardware, we present an alternative dynamical formulation where the forward drive and Jacobian operators are evaluated individually at \mathbf{x} and \mathbf{z} rather than at the shared midpoint, neglecting all non-linear orders of the stress term $(\mathbf{x} - \mathbf{z})$ in Eq.(10). One can easily see that only the linear term of the stress term $(\mathbf{x} - \mathbf{z})$ will contribute to the gradient.

D.1. Split-Dynamics Equations

Using the same notation of the main text, neglecting all non-linear orders of $(\mathbf{x} - \mathbf{z})$ in Eq.(10), we get

$$\frac{d\mathbf{x}}{dt} = \frac{1}{2} \left[F(\mathbf{x}) + F(\mathbf{z}) \right] + \frac{1}{2} \mathbf{J}(\mathbf{x})(\mathbf{x} - \mathbf{z}) + \frac{1}{2} \nabla_{\mathbf{x}} C, \quad (42)$$

$$\frac{d\mathbf{z}}{dt} = \frac{1}{2} \left[F(\mathbf{x}) + F(\mathbf{z}) \right] - \frac{1}{2} \mathbf{J}(\mathbf{z})(\mathbf{x} - \mathbf{z}) - \frac{1}{2} \nabla_{\mathbf{z}} C. \quad (43)$$

Here, $\nabla_{\mathbf{u}} C$ denotes the gradient of the loss injected at the output block of the state \mathbf{u} .

This formulation avoids the computation of the midpoint state \mathbf{m} for derivative evaluations.

Algorithm 3 Decoupled Split-Jacobian \mathbf{x} - \mathbf{z} Relaxation

```

1: Input:  $\mathbf{x}_0, \mathbf{y}$ , parameters  $\{\mathbf{W}_\ell, \mathbf{b}_\ell\}_{\ell=1}^L$ , step size  $\eta > 0$ ,  

   tolerance  $\varepsilon > 0$ 
2: Initialize  $\mathbf{x}^0 = \mathbf{0}, \mathbf{z}^0 = \mathbf{0}$ 
3: for  $k = 0, 1, 2, \dots$  do
4:   Define local variables:
     $\mathbf{s}^k = \mathbf{x}^k - \mathbf{z}^k,$   

     $\Sigma^k = \frac{1}{2} [\sigma(\mathbf{W}\mathbf{x}^k + \beta) + \sigma(\mathbf{W}\mathbf{z}^k + \beta)],$   

     $\mathbf{D}_x^k = \text{diag}(\sigma'(\mathbf{W}\mathbf{x}^k + \beta)), \quad \mathbf{g}_x^k = \nabla_{\mathbf{x}} C(\mathbf{x}^k, \mathbf{y}),$   

     $\mathbf{D}_z^k = \text{diag}(\sigma'(\mathbf{W}\mathbf{z}^k + \beta)), \quad \mathbf{g}_z^k = \nabla_{\mathbf{z}} C(\mathbf{z}^k, \mathbf{y}).$ 
5:   Compute velocity fields (fully decoupled dynamics):
     $\dot{\mathbf{x}}^k = \Sigma^k - \mathbf{x}^k + \frac{1}{2} \mathbf{W}^\top \mathbf{D}_x^k \mathbf{s}^k + \frac{1}{2} \mathbf{g}_x^k,$   

     $\dot{\mathbf{z}}^k = \Sigma^k - \mathbf{z}^k - \frac{1}{2} \mathbf{W}^\top \mathbf{D}_z^k \mathbf{s}^k - \frac{1}{2} \mathbf{g}_z^k$ 
6:   Update states:
     $\mathbf{x}^{k+1} \leftarrow \mathbf{x}^k + \eta \dot{\mathbf{x}}^k, \quad \mathbf{z}^{k+1} \leftarrow \mathbf{z}^k + \eta \dot{\mathbf{z}}^k$ 
7:   if  $\|\mathbf{x}^{k+1} - \mathbf{x}^k\|_2 + \|\mathbf{z}^{k+1} - \mathbf{z}^k\|_2 < \varepsilon$  then
8:     break
9:   end if
10:  end for
11:  Equilibrium variables:
     $\bar{\mathbf{m}} = \frac{1}{2}(\mathbf{x}^k + \mathbf{z}^k), \quad \bar{\mathbf{s}} = \mathbf{x}^k - \mathbf{z}^k.$ 
12:  Gradient computation:
    
$$\frac{dC}{d\mathbf{W}} = \mathbf{D}(\bar{\mathbf{m}}) \bar{\mathbf{s}} \bar{\mathbf{m}}^\top.$$


```

D.2. Split-Jacobian Relaxation Algorithm

The corresponding discrete-time implementation of the Split-Dynamics is provided in Algorithm 3. This reformulation of the algorithm, tested on the same tasks, matches the performance of algorithm 1 as predicted from the theory.

E. Additional Experimental Results

In this section, we provide additional experimental results corroborating the gradient fidelity of the proposed Algorithm 1. We compare the relaxation-derived gradients against reference gradients computed via standard backpropagation (BP) on the CIFAR-10 dataset.

E.1. Training Stability and Loss Trajectory

To validate that the relaxation dynamics do not introduce optimization artifacts, we tracked the training loss across

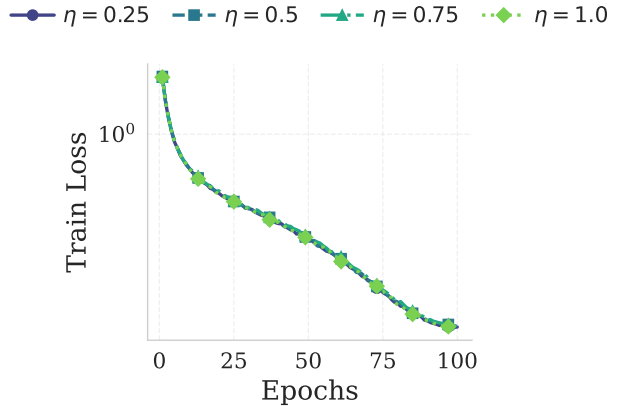


Figure 3. Training Loss Consistency. The decay of training loss for the relaxation algorithm matches exactly across all step sizes. Axes indicate Epochs (0–100) versus Loss (log scale).

different Euler step sizes η . As illustrated in Figure 3, the learning trajectories for $\eta \in \{0.25, 0.5, 0.75, 1.0\}$ indistinguishably overlap with the ideal case $\eta = 1$. This further confirms that the saddle-point formulation effectively solves the credit assignment problem without degrading optimization stability.

E.2. Gradient Norm Consistency

A critical requirement for replacing symbolic differentiation with physical relaxation is the preservation of gradient magnitude. We measured the norm ratio $\|\nabla_{\text{relax}}\|/\|\nabla_{\text{BP}}\|$ throughout training.

Figure 4 demonstrates that the proposed method maintains near-perfect scale consistency. The deviation from unity is negligible, with fluctuations bounded within a minute range of 0.0001 to -0.0003. This confirms that the stress variable $\mathbf{s} = \mathbf{x} - \mathbf{z}$ correctly accumulates the total sensitivity of the loss with respect to activations.

E.3. Directional Alignment

We can also observe that the directional accuracy of the gradient update is paramount. We present here a global quantification of this using the global cosine misalignment metric, defined as $1 - \cos(\theta)$, where θ is the angle between ∇_{relax} and ∇_{BP} as measured in the main text.

Figure 5 reveals that the misalignment is practically zero. The metric consistently falls below 10^{-5} oscillating around 10^{-7} , confirming to be almost indistinguishable from standard backpropagation (the accuracy used in the code is IEEE 754 Float32single point precision corresponding to a decimal precision $\approx 10^{-7}$).

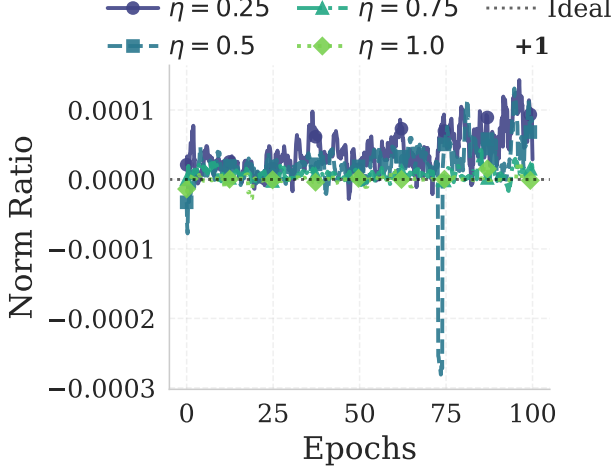


Figure 4. Gradient Norm Fidelity. The ratio between the norms of relaxation gradients and backpropagation gradients remains centered at 1.0, with deviations smaller than 10^{-4} . Legend indicates step sizes $\eta = 0.25$ through $\eta = 1.0$.

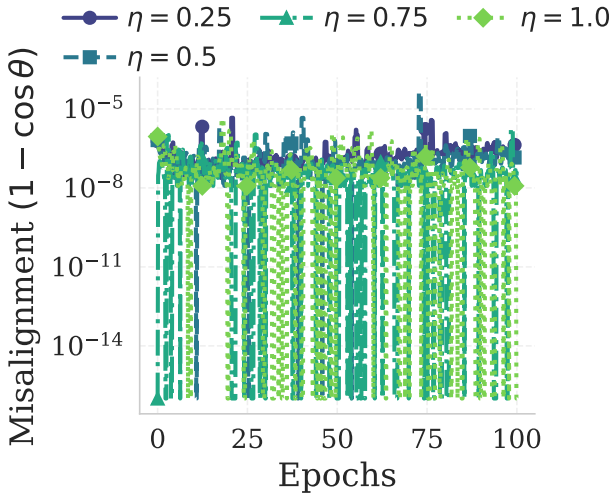


Figure 5. Directional Alignment. The cosine misalignment ($1 - \cos \theta$) between the relaxation algorithm and standard BP.

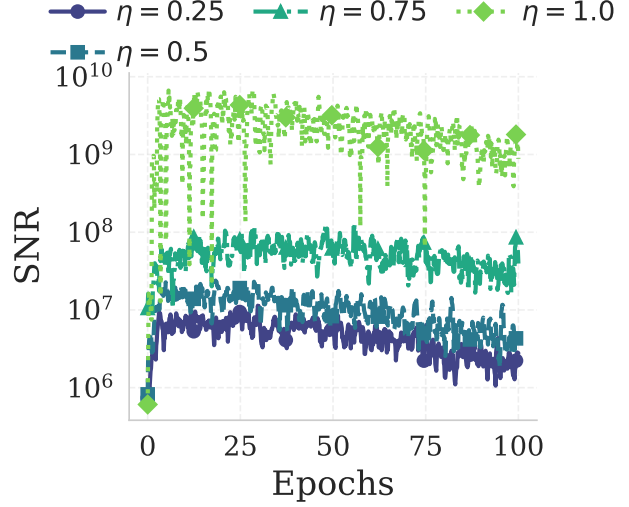


Figure 6. Gradient Signal-to-Noise Ratio. The SNR consistently exceeds 10^6 , confirming that the relaxation error is negligible compared to the gradient signal.

E.4. Signal-to-Noise Ratio (SNR)

Finally, we assessed the quality of the gradient estimator by computing the Signal-to-Noise Ratio (SNR), defined as $\|\nabla_{\text{BP}}\|^2 / \|\nabla_{\text{relax}} - \nabla_{\text{BP}}\|^2$.

As shown in Figure 6, the SNR remains exceptionally high throughout the training process, consistently exceeding 10^6 (60 dB) and peaking near 10^9 . We observe a non-linear relationship where larger step sizes (e.g., $\eta = 1.0$) yield much higher SNR.

E.5. Layer-wise Misalignment and Time Step

In our experimental analysis, we observed that while the overall gradient accuracy remains exceptionally high, a subtle degradation in alignment emerges as signals propagate backward to earlier layers (e.g., Layer 1) over the course of training. This phenomenon is visualized in Figure 7, which displays the log-misalignment for a step size of $\eta = 0.25$. This slight drift is attributable to the propagation of numerical errors inherent to the finite-time step approximation of the continuous dynamics.

Conversely, using the theoretically optimal step size $\eta = 1.0$ (Figure 8) recovers perfect alignment across all layers. We stress that digital implementation is not our goal; these experiments serve simply to demonstrate consistency and experimentally validate the theory.

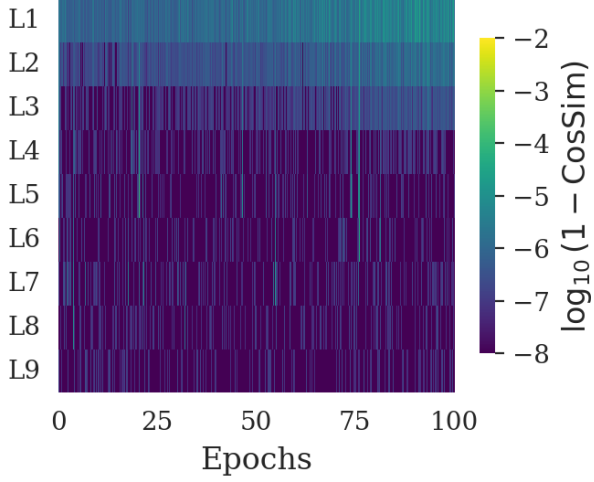
Layer Misalignment ($\eta = 0.25$)

Figure 7. **Log-misalignment heatmap** ($\eta = 0.25$). The plot displays $\log_{10}(1 - \text{CosSim})$ for each layer. A minor accumulation of numerical error is visible in earlier layers, consistent with finite-step approximations.

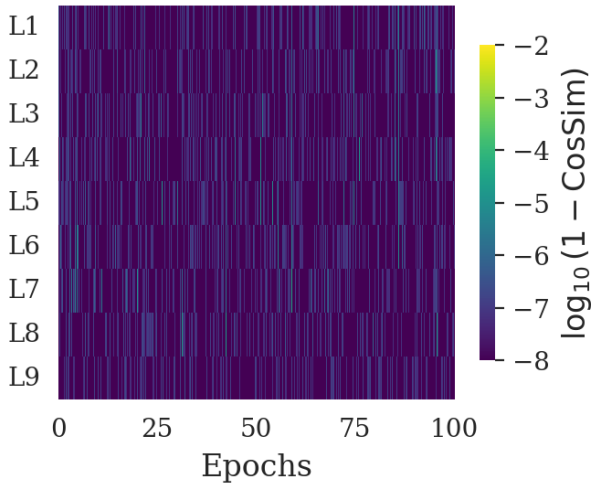
Layer Misalignment ($\eta = 1.0$)

Figure 8. **Log-misalignment heatmap** ($\eta = 1.0$). The plot displays $\log_{10}(1 - \text{CosSim})$ for each layer. The alignment is effectively perfect (bounded only by machine precision), confirming that the unit-step discretization recovers the exact gradient.